

# On the Effect of Human Arm Manipulability in 3D Force Tasks: Towards Force-controlled Exoskeletons

Panagiotis K. Artemiadis, Pantelis T. Katsiaris, Minas V. Liarokapis, and Kostas J. Kyriakopoulos

**Abstract**—Coupling the human upper limbs with robotic devices is gaining increasing attention in the last decade, due to the emerging applications in orthotics, prosthetics and rehabilitation devices. In the cases of every-day life tasks, force exertion and generally interaction with the environment is absolutely critical. Therefore, the decoding of the user’s force exertion intention is important for the robust control of orthotic robots (e.g. arm exoskeletons). In this paper, the human arm manipulability is analyzed and its effect on the recruitment of the musculo-skeletal system is explored. It was found that the recruitment and activation of muscles is strongly affected by arm manipulability. Based on this finding, a decoding method is built in order to estimate force exerted in the three-dimensional (3D) task space from surface ElectroMyoGraphic (EMG) signals, recorded from muscles of the arm. The method is using the manipulability information for the given force task. Experimental results were verified in various arm configurations with two subjects.

## I. INTRODUCTION

Coupling the human upper limb with robotic devices is gaining increasing attention in the last decade, due to the emerging applications in orthotics, prosthetics and rehabilitation devices. In these applications, the devices are worn by the subjects, who can either use them for executing demanding tasks (i.e. power augmentation) or for supporting them during the execution of every-day life tasks in cases of subjects with motor impairments. Interaction with the environment is however critical, and in most cases it entails the exertion of force to the environment, transmitted through the worn device. Therefore, it is necessary to be able to infer the user’s intention in terms of force exertion, in order to be able to control the robotic device robustly and safely.

Decoding the intention of force exertion has been realized mainly using surface ElectroMyoGraphic (EMG) signals from the arm muscles. A myokinetic arm model for estimating joint torque from EMG signals during maintained posture was presented in [1]. This model was based on anatomical and physiological data to estimate joint torques from EMG. However, the model was limited to maintained posture in planar arm configurations. An index of muscle quasi-tension calculated from EMG signals that was used

for estimating arm stiffness was presented in [2], but again the configurations tested were only on the plane, while a continuous profile of force was not estimated through EMG. The authors have used EMG signals from four muscles of the arm in order to compute force exerted in planar motion in the past [3], however the arm configurations tested were limited, while again the arm was restricted on a plane parallel to the human transverse plane.

The human arm is definitely a quite complex mechanism, with a highly redundant structure both in kinematic and actuation level. A large number of muscles (approximately 30) actuate the shoulder, elbow, and wrist joints, while the kinematic redundancy is used for improving dexterity during the execution of complicated motion and/or force tasks. However, one can easily argue that humans learn to execute specific tasks in a certain way, while whether it’s the “optimum” way or not is still under investigation. Focusing on force tasks, humans learn to interact with the environment quite easily, and once “trained”, they don’t significantly vary their strategy [4]. Therefore, the way humans choose to interact with the environment could be a combination of variables related to the redundancy in both motor and kinematic level.

In this paper, the force manipulability, thereafter mentioned as manipulability for simplicity, of the human upper limb is analyzed for force tasks in the three-dimensional (3D) workspace. Manipulability is a measure of the force exertion capability of the arm along the axes of the given task, and is dependent on arm configuration [5]. Multiple force exertion tasks are executed by two subjects in different arm configurations, along a variety of directions. The muscular activity of the corresponding muscles is recorded and analyzed with respect to the force execution capability of the arm as described by the manipulability, for a given configuration and force task. Results show that arm manipulability plays a significant role in the execution of the force task, affecting the recruitment of the muscles and their activity. Using this result, a decoding algorithm is created to transform EMG signals to a continuous representation of exerted force along the three axes of the workspace. The proposed method is tested with two subjects in many different configurations covering a wide portion of the arm workspace.

The rest of the paper is organized as follows: Section II analyzes the procedures and experimental methods and algorithms used, Section III presents the results on the manipulability effects on force tasks and the decoding of exerted forces, while Section IV concludes the paper.

P. K. Artemiadis is with the Department of Mechanical Engineering, Massachusetts Institute of Technology (MIT), Cambridge, MA, USA. Email: [partem@mit.edu](mailto:partem@mit.edu).

P. T. Katsiaris, M. V. Liarokapis and K. J. Kyriakopoulos are with the Control Systems Lab, School of Mechanical Eng., National Technical University of Athens, 9 Heron Polytechniou Str, Athens, 157 80, Greece. Email: [pkatsiar@mail.ntua.gr](mailto:pkatsiar@mail.ntua.gr), [mliaro@mail.ntua.gr](mailto:mliaro@mail.ntua.gr), [kkyria@mail.ntua.gr](mailto:kkyria@mail.ntua.gr).

This work has been partially supported by the European Commission with the Integrated Project no. 248587, “THE Hand Embodied”, within the FP7-ICT-2009-4-2-1 program “Cognitive Systems and Robotics”.

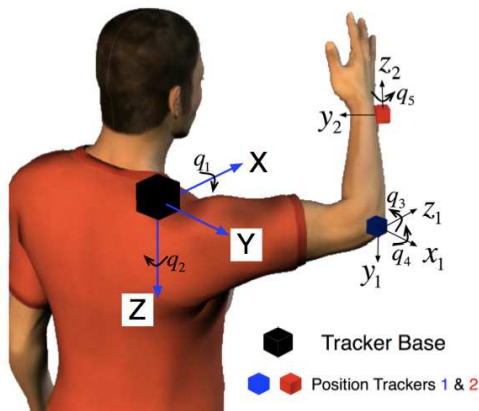


Fig. 1. Definition of the 5 modelled joint angles for the shoulder and elbow.

## II. METHODS

### A. Rationale and requirements

There is no doubt that the kinematic structure of the human upper extremity is quite efficient, while very complex. Narrowing our interest down to the upper limb and not considering finger motion, the kinematics of the arm can be modeled with 7 degrees of freedom, which leads to the definition of human arm redundancy. The latter however is not only exploited in performing arm motions in the 3D space, but also in interacting with the environment, where forces are exerted. In other words, arm configuration is appropriately selected based on the force tasks to be executed. In order to quantify the force exertion capability, we use the measure of manipulability. Briefly, if  $\tau \in \mathbb{R}^n$  the vector of joint torques for a series manipulator with  $n$  degrees of freedom (DoFs), then a unity sphere in the joint torque space is described by  $\tau^T \tau = 1$ . The latter, accounting for  $\tau = \mathbf{J}^T(\mathbf{q}) \mathbf{h}$ , where  $\mathbf{q}$  is the joint angle vector,  $\mathbf{J}^T(\mathbf{q})$  is the Jacobian matrix and  $\mathbf{h}$  is the vector of the forces at the end-effector, is mapped into the ellipsoid in the space of end-effector forces as shown below:

$$\mathbf{h}^T (\mathbf{J}(\mathbf{q}) \mathbf{J}^T(\mathbf{q})) \mathbf{h} = 1. \quad (1)$$

Equation 1 defines the force manipulability ellipsoid, thereafter mentioned as manipulability ellipsoid for simplicity. This ellipsoid characterizes the end-effector forces that can be generated with the given set of joint torques, with the manipulator in a given posture [5].

In this study, we focused on the principal joints of the upper limb, i.e. the shoulder and the elbow. The wrist motion was not included in the analysis for simplicity. Therefore, 5 degrees of freedom were analyzed; shoulder abduction-adduction, shoulder flexion-extension, shoulder external-internal rotation, elbow flexion-extension and forearm pronation-supination, which can be simulated by 5 corresponding joint angles, i.e.  $q_1, q_2, q_3, q_4, q_5$  for the human arm, as shown in Fig. 1. For more details on the kinematics the reader should refer to [6].

Following the notation in (2), in our case  $\mathbf{h} = [F_x \ F_y \ F_z]^T$  where  $F_x, F_y, F_z$  the forces exerted to

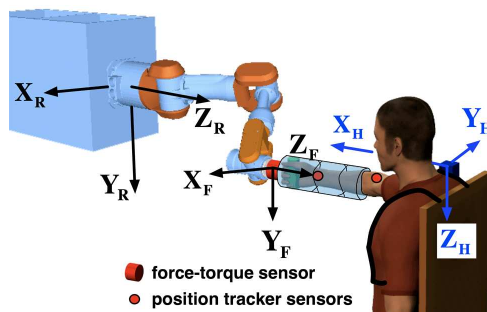


Fig. 2. The experimental setup.

the environment along the three corresponding axes  $\mathbf{X}_H, \mathbf{Y}_H, \mathbf{Z}_H$  as shown in Fig. 2,  $\mathbf{J}(\mathbf{q}) \in \mathbb{R}^{3 \times 5}$  is the Jacobian matrix, and  $\tau \in \mathbb{R}^5$  is the vector of joint torques at the corresponding human joints modelled. Therefore, the ellipsoid described by (1) can be drawn in the 3D space, for each configuration of the human arm. Along the direction of the major axis of the ellipsoid the human arm can exert larger forces, than along the direction of the minor axes. Let  $\mathbf{x}_{(1)}, \mathbf{x}_{(2)}, \mathbf{x}_{(3)} \in \mathbb{R}^3$  be the axes of the ellipsoid which are given by:

$$(\lambda_i \mathbf{I} - (\mathbf{J}(\mathbf{q}) \mathbf{J}^T(\mathbf{q}))) \mathbf{x}_{(i)} = \mathbf{0}, \quad i = 1, 2, 3 \quad (2)$$

where  $\lambda_i$  are the eigenvalues of the matrix  $\mathbf{J}(\mathbf{q}) \mathbf{J}^T(\mathbf{q})$ . The principal axis of the ellipsoid is the one corresponding to the larger eigenvalue.

Since the human motor control seems to exploit redundancy not only for kinematic control but also for interacting with the environment, this study focused on how the ability to exert forces given a configuration (as described by the force manipulability ellipsoid), affects the recruitment and activity of the force sources of the human arm, i.e. the skeletal muscles. Therefore, an experimental platform is needed to be able to measure exerted forces and muscle activity for a variety of different arm configurations, and compare them based on the manipulability ellipsoids for each configuration. The purpose of this work however was not to investigate how humans choose their arm configuration according to the task force requirements, but given a preferred arm configuration, what is the effect of the manipulability ellipsoid on the activation of the musculoskeletal system.

### B. Apparatus

The experimental setup included subjects holding a handle mounted on the end-effector of a 7 DoFs robot arm. Subjects were seated with their trunk restrained to a chair through harness belt. The subjects gripped an appropriately designed handle, mounted on the robot end-effector, with their dominant arm (the right arm for all subjects participated). The handle was inside a tube, in which the subject's forearm was inserted. The subjects' forearm was supported inside the tube through elastic straps transversely inserted into the tube. The tube was appropriately designed so that it restrained wrist motion (wrist flexion-extension and radial-ulnar deviation). The subjects were instructed to always hold the handle firmly. The handle-tube along with the subjects' hand is graphically

depicted in Fig. 2. A 7-DoF robot arm, equipped with a force-torque sensor at its end-effector, was used to generate motion perturbations to the human arm, through the tube-handle system shown. The tube was firmly connected with the force-torque sensor. Position tracker sensors were also placed at the elbow and the wrist of the user, while the reference system was attached on the shoulder of the user.  $\mathbf{X}_R, \mathbf{Y}_R, \mathbf{Z}_R$  are the robot reference frame axes.  $\mathbf{X}_H, \mathbf{Y}_H, \mathbf{Z}_H$  are the human (or position tracker) reference frame axes.  $\mathbf{X}_F, \mathbf{Y}_F, \mathbf{Z}_F$  are the force-torque sensor reference frame axes.

The tube-handle system was mounted on a 7-DoF robot manipulator (PA-10, Mitsubishi Heavy Industries). The robot arm can be controlled in joint space, either in position or in torque, while feedback for position and torque at each joint is available in real time. Further information for hardware characteristics, kinematics and dynamics can be found in [7]. Between the tube-handle mounting and the robot end-effector, a 6-axis force-torque sensor (JR3 Inc.) was included for measuring human-robot interaction forces in the three axes of space. The subjects were placed facing the robot from a distance so that most of their arm workspace<sup>1</sup> was accessible from the robot workspace. Fig. 2 depicts the experimental setup.

A magnetic position tracking system (Isotrak II, Polhemus Inc) was used for measuring the human arm configuration. The position tracking system was equipped with a base reference system, with respect to which, the 3D-position and orientation of two small position sensors is given in real-time. The size of the position sensors was 2.83(W) 2.29(L) 1.51(H) cm, and they were firmly attached at the elbow (at the olecranon) and the wrist (at the styloid process of radius) of the subject, while the reference system was placed on the subjects' shoulder as shown in Fig. 1. The axes of the robot arm and position tracking system were properly aligned during a calibration procedure, using online measurements of both systems. Let  $\mathbf{X}_R, \mathbf{Y}_R, \mathbf{Z}_R$  be the robot reference axes vectors, and let  $\mathbf{X}_H, \mathbf{Y}_H, \mathbf{Z}_H$  be the human references axes vectors (i.e. the position tracking system base). Then, the relationship between them, as shown in Fig. 2, is defined by

$$\begin{bmatrix} \mathbf{X}_R & \mathbf{Y}_R & \mathbf{Z}_R \end{bmatrix} = \begin{bmatrix} -\mathbf{Y}_H & \mathbf{Z}_H & -\mathbf{X}_H \end{bmatrix} \quad (3)$$

Finally, using the tracker position and orientation measurements, the modelled joint angles were computed through inverse kinematics. The inverse kinematic equations are omitted for simplicity, while the reader should refer to [6] for further analysis.

The position tracking system along with the servo-controller of the robot arm were interfaced with a personal computer (PC) running Linux through serial communication (RS-232) and ARCNET protocols respectively. The force-torque sensor measurements were collected using the appropriate measurement PCI board mounted on the same PC. The robot arm control frequency was 500 Hz, the force-torque measurement frequency was also 500 Hz, while the

<sup>1</sup>The subjects' trunk and behind this point were out of the workspace of the robot arm for safety.

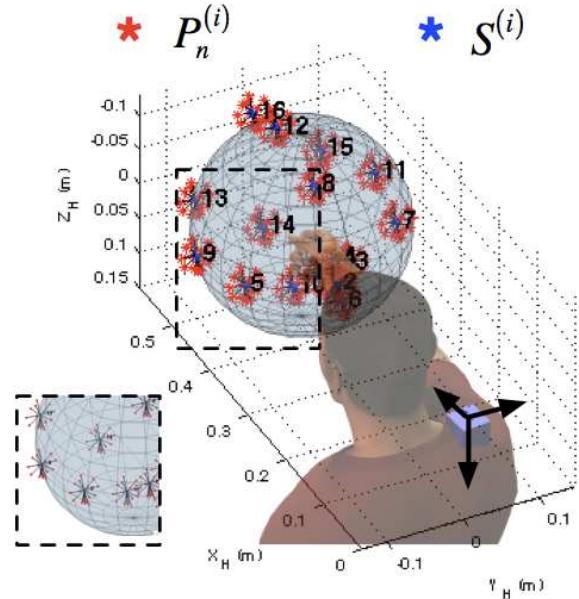


Fig. 3. Starting points,  $S^{(i)}$ ,  $i = 1, 2, \dots, 16$ , and corresponding target points,  $P_n^{(i)}$ ,  $n = 1, 2, \dots, 16$ , for end-point perturbation in the 3D arm workspace. All the starting points lie on a sphere. A close-up of a part of the sphere, with some starting points lying on it, is shown at the bottom left side.

position tracker provided measurements at 30 Hz. Data from the position tracker were re-sampled offline at 500 Hz, using an anti-aliasing FIR filter (low-pass, order: 24, cut-off frequency: 100 Hz).

EMG signals were acquired using a signal acquisition board (NI-DAQ 6036E, National Instruments) connected to an EMG system (Bagnoli-16, Delsys Inc.). Single differential surface EMG electrodes (DE-2.1, Delsys Inc.) were used. The main responsible muscles for the chosen task were recorded: deltoid (anterior), deltoid (middle), pectoralis major, trapezius descendens (upper), biceps brachii, brachio-radialis, triceps brachii (long head). The EMG recordings from each muscle were preprocessed using the linear envelop technique, i.e. full-wave rectified, low-pass filtered and normalized to their maximum voluntary isometric contraction (MVC) value [8]. MVC values for all muscles were acquired using guidelines found in [9].

### C. Procedures and Tasks

Two subjects participated in the experiments. Each subject was asked to firmly hold the handle while looking towards the robot arm, as shown in Fig. 2. The robot arm end-effector was initially positioned at 16 starting 3D points ( $S^{(i)}$ ,  $i = 1, 2, \dots, 16$ ), inside the human arm workspace. More specifically, the starting points belonged to a sphere of radius 20 cm and center a point chosen as the center of studied arm workspace<sup>2</sup>. Starting from each point  $S^{(i)}$ ,

<sup>2</sup>The center of the studied human arm workspace was chosen at a point at the height of subjects chest, on the sagittal plane, at an approximate distance of 40 cm from the coronal plane. The latter choice was not based on any physiologically defined point. It was selected to allow studying a wide range of the available human arm workspace, while guaranteeing the safety of the subjects.

the robot end-effector was moved to 16 surrounding points  $P_n^{(i)}$ ,  $n = 1, 2, \dots, 16$ , that belonged to a sphere with center the point  $S^{(i)}$  and radius equal to 3 cm. All the points and motion paths are depicted in Fig. 3.

The robot end-effector initiated the motion from each point  $S^{(i)}$ ,  $i = 1, 2, \dots, 16$ , to each point  $P_n^{(i)}$ ,  $n = 1, 2, \dots, 16$ , lasting for 3 seconds (*center-out phase*). After arriving at point  $P_n^{(i)}$ , the robot stayed there for 2 seconds (*relax phase 1*), and then returned to the starting point  $S^{(i)}$  following a constant velocity line path taking 2 seconds (*return phase*). Finally the robot end-effector stayed there for 2 seconds (*relax phase 2*), before initiating motion for the next  $P_{n+1}^{(i)}$  point. The subjects were instructed to try to maintain their hand initial position  $S^{(i)}$  only during the *center-out phase*, i.e. trying to restrain to robot center-out motion. During all the other phases (*relax phase 1* and *2*, and *return phase*) the subjects were instructed to relax and passively follow robot induced motion.

The perturbed motion coming from the robot end-effector motion during the *center-out phase* was specifically designed as sinusoidal, producing a variety of exerted force magnitudes. More specifically, the sinusoidal trajectory was designed so that the robot end-effector was performing two full-periods of sinusoidal oscillations around the initial point  $S^{(i)}$ , along each axis of motion. The amplitude of the sinusoidal motion was equal to the distance between the initial point  $S^{(i)}$  and the target point  $P_n^{(i)}$ , while the duration of sinusoidal motion was three seconds, succeeded by the two-second resting period (*relax phase 1*). Let  $S^{(i)} = \begin{bmatrix} x_0^{(i)} & y_0^{(i)} & z_0^{(i)} \end{bmatrix}^T$  and  $P_n^{(i)} = \begin{bmatrix} x_{nf}^{(i)} & y_{nf}^{(i)} & z_{nf}^{(i)} \end{bmatrix}^T$  be the coordinates of the starting and the surrounding points with respect to the robot base reference system. The sinusoidal trajectory  $\begin{bmatrix} x_{sn}^{(i)}(t) & y_{sn}^{(i)}(t) & z_{sn}^{(i)}(t) \end{bmatrix}^T$  along each axis  $\mathbf{X}_R$ ,  $\mathbf{Y}_R$ ,  $\mathbf{Z}_R$  respectively, was given by:

$$\begin{bmatrix} x_{sn}^{(i)}(t) \\ y_{sn}^{(i)}(t) \\ z_{sn}^{(i)}(t) \end{bmatrix} = \begin{bmatrix} x_0^{(i)} \\ y_0^{(i)} \\ z_0^{(i)} \end{bmatrix} + \begin{bmatrix} x_{nf}^{(i)} - x_0^{(i)} \\ y_{nf}^{(i)} - y_0^{(i)} \\ z_{nf}^{(i)} - z_0^{(i)} \end{bmatrix} \sin\left(\frac{4\pi}{3}t\right) \quad (4)$$

where  $t$  represents time, and  $t = 0$  denotes the start of the *center-out phase* for each of the surrounding points  $P_n^{(i)}$ .

Therefore, the 3D position of the robot end-effector at each time instance was defined by the sinusoidal trajectory in (4). Regarding the orientation, the robot end-effector was controlled to have all orientation angles (roll, pitch and yaw) equal to zero. This essentially guaranteed that the tube-handle system would keep a constant orientation with respect to the subject, which was identical to the initial one, as shown in Fig. 2<sup>3</sup>. Having the desired pose of the robot end-effector, the appropriate robot joint angles were computed using the pseudo-inverse Jacobian method [5]. For details on this procedure, the reader can refer to [7]. All the robot trajectories were designed and computed offline. Having computed the desired robot trajectories in joint space,

<sup>3</sup>The tube longitudinal axis was always perpendicular to the coronal plane.

the robot could be commanded to track those trajectories using its high performance servo controller, with a maximum tracking error in joint space that did not exceed 0.02 deg. Finally, the force-torque sensor was mounted on the robot end-effector, while its axes were aligned to those of the robot, as shown in Fig. 2.

Each of the two subjects (2 males of 25 and 26 years old respectively) completed the experimental session including the 16 surrounding target  $P_n^{(i)}$ ,  $n = 1, 2, \dots, 16$ , for each of the 16 starting points  $S^{(i)}$ ,  $i = 1, 2, \dots, 16$  inside their arm workspace. The recording of the data started as soon as the robot end-effector initiated motion from each of the points  $S^{(i)}$ ,  $i = 1, 2, \dots, 16$  to its surrounding targets  $P_n^{(i)}$ ,  $n = 1, 2, \dots, 16$ . For example, if  $t = 0$  is when the robot initiated motion from point  $S^{(1)}$  to each one of its 16 surrounding targets  $P_1^{(1)}, P_2^{(1)}, \dots, P_{16}^{(1)}$ , then the experiment stops after 16 motions from  $S^{(1)}$  to each  $P_n^{(1)}$ ,  $n = 1, 2, \dots, 16$  and back to  $S^{(1)}$ , lasting eventually  $t = 9 * 16 = 144sec$ . Then the robot was moved to the next initial point (i.e.  $S^{(2)}$ ) and the next session was started as soon as the subject confirmed that he was ready after resting his arm. All experimental procedures were conducted under a protocol approved by the National Technical University of Athens Institutional Review Board.

### III. RESULTS

#### A. Manipulability and musculoskeletal system

Let  $t_i^n$  denote each trial, during which, the robot end-effector initiated the motion from each point  $S^{(i)}$ ,  $i = 1, 2, \dots, 16$ , to each point  $P_n^{(i)}$ ,  $n = 1, 2, \dots, 16$ , while the subject was exerting opposing forces along the direction of the motion of the end-effector. Moreover, for each point  $S^{(i)}$ ,  $i = 1, 2, \dots, 16$ , the human arm configuration  $\mathbf{q}_i \in \mathbb{R}^5$  was computed from the position tracking system. Since the surrounding points  $P_n^{(i)}$  to each  $S^{(i)}$  were very close, the arm configuration is assumed to be constant throughout each trial  $t_i^n$ . Knowing the arm configuration, we could compute the manipulability ellipsoid for each trial. Moreover, knowing the path of the robot end-effector, the direction of the induced motion for each trial could also be computed. Let  $\mathbf{p}_i^n$  denote a unit vector along the direction of motion for trial  $t_i^n$ , starting from  $S^{(i)}$ . Let  ${}^n\mathbf{x}_{(1)}$ ,  ${}^n\mathbf{x}_{(2)}$ ,  ${}^n\mathbf{x}_{(3)}$  be the axes of the manipulability ellipsoids, where  ${}^n\mathbf{x}_{(1)}$  the major axis. Then, a measure of alignment within the vector  $\mathbf{p}_i^n$  and each of the axes  ${}^n\mathbf{x}_{(1)}$ ,  ${}^n\mathbf{x}_{(2)}$ ,  ${}^n\mathbf{x}_{(3)}$ , defined by  ${}^nA_1$ ,  ${}^nA_2$ ,  ${}^nA_3$  respectively, was computed by:

$${}^nA_k = \frac{\mathbf{p}_i^n \cdot {}^n\mathbf{x}_{(k)}}{\|{}^n\mathbf{x}_{(k)}\|}, \quad k = 1, 2, 3 \quad (5)$$

where  $(\cdot)$  denotes the vectors inner product. The alignment measures  ${}^nA_k$ ,  $k = 1, 2, 3$  take value at the range  $[-1, 1]$ , while the closer its absolute value is to 1, the more the vector  $\mathbf{p}_i^n$  is aligned to the corresponding axis of the manipulability ellipsoid. The values of the alignment measure  ${}^nA_k$ ,  $k = 1, 2, 3$ , for all trials (i.e.  $16 \times 16 = 256$  trials) were computed for each subject.



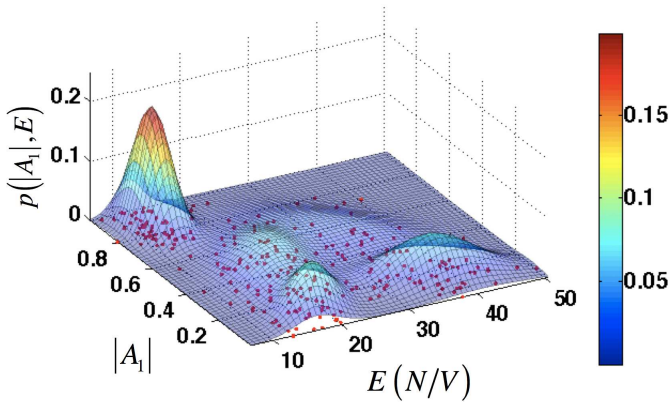


Fig. 4. Measure of muscular effort  $E$  with respect to the absolute value  $|A_1|$  of the alignment measure with the manipulability ellipsoid major axis. The measured points (red dots) and a fitted probability density function for their joint probability distribution  $p(|A_1|, E)$  are shown. A Gaussian Mixture Model with 5 components was used for fitting the joint probability distribution [10].

Among all trials, the magnitude of applied force could be assumed as similar, since the subjects were instructed to withstand to the robot induced motion equally across the workspace. However, in order to quantify the effort “paid” for each trial, the muscular activity was also used. The integral of the EMG signals after preprocessing them (using the linear envelop technique) was computed for each muscle, for each trial. Let  ${}^n U$  be the sum of those integrals for the trial  $t_i^n$ . Then, we defined a measure of effort  ${}^n E$ , for each trial  $t_i^n$ , as the quotient of the integral of the total force applied through the trial to the muscle effort represented by  ${}^n U$ , i.e.

$${}^n E = \frac{{}^n F_{int}}{{}^n U} \quad (6)$$

The computed values of the measure of effort  ${}^n E$  are plotted with respect to the absolute value of the alignment measure  ${}^n |A_1|$  for all trials in Fig. 4. Moreover, a fitted probability distribution function is also drawn. As it can be seen, the muscular effort was less in the cases where the absolute alignment measure with the ellipsoid major axis was close to 1, i.e. when the direction of the exerted force was closer to the direction of the manipulability ellipsoid major axis. Finally, it must be noted that we chose the aforementioned way to describe muscular effort, while many other variables or measures could have been used.

### B. Decoding 3D force from EMG

Based on the effect of the manipulability on the effort of muscles during force exertion, as analyzed above, we built a decoding algorithm to estimate arm exerted forces along the 3 axes of the arm workspace. The decoding scheme included the information about the alignment of the major axis of the manipulability ellipsoid (for a given arm configuration) with the direction of the exerted force. Given the alignment measure between the two vectors as described in (5), a set of linear decoding models was trained. Each member (decoding model) of this set was trained using only data of muscle activations and exerted forces which had similar alignment measures. The method is described below.

The inputs to the decoder were the processed muscle activations. The muscles activations were represented in a low-dimensional space, by using the Principal Component Analysis (PCA) method for reducing the data space. A three dimensional space was finally selected for representing the 7 muscles’ activation. Details on the algorithm application on EMG data can be found in [11], [12]. The output of the decoder were the estimates of the continuous representation of the force vector magnitude in 3D space. The training data were grouped in subsets, each one of which included data (inputs and outputs) for experiments with similar to each other alignment measures. The absolute value of the later was used, and the resulted range  $[0, 1]$  was sectioned in 10 subsets with equal width (0.1). For each of the subsets, a linear hidden-state model was trained and used for decoding. A linear hidden-state model is described by the following set of equations:

$$\begin{aligned} \mathbf{x}_{t+1} &= \mathbf{G}_i \mathbf{x}_t + \mathbf{B}_i \mathbf{U}_t + \mathbf{v}_t \\ \mathbf{F}_t &= \mathbf{C}_i \mathbf{x}_t + \mathbf{w}_t \end{aligned} \quad (7)$$

where  $\mathbf{x}_t \in \mathbb{R}^d$  is a hidden state vector,  $d$  is the dimension of this vector and  $\mathbf{v}_t$ ,  $\mathbf{w}_t$  are zero-mean Gaussian noise variables in process and observation equations respectively, i.e.  $\mathbf{v}_t \sim N(\mathbf{0}, \mathbf{V}_i)$ ,  $\mathbf{w}_t \sim N(\mathbf{0}, \sigma_i)$ , where  $\mathbf{V}_i \in \mathbb{R}^{d \times d}$ ,  $\sigma_i \in \mathbb{R}$  are the covariance matrix and variance of  $\mathbf{v}_t$ ,  $\mathbf{w}_t$  respectively. Matrices  $\mathbf{G}_i$  ( $d \times d$ ),  $\mathbf{B}_i$  ( $d \times 3$ ) and  $\mathbf{C}_i$  ( $1 \times d$ ) represented the dynamics of the hidden states, the relation between the low dimensional embeddings of muscles activation ( $\mathbf{U}$ ) and the hidden states dynamics, and the relation of the hidden states to the output variable of the model respectively. The output variable of the decoding model is the magnitude of the exerted force  $\mathbf{F}$ . The size  $d$  of the hidden state vector for each model was chosen using the Akaike criterion [13]. The subscript  $i$  in the model parameters denotes the different models for each of the 10 subsets based on the manipulability alignment measure, as defined below. Linear hidden-state models of similar form were used by the authors in the past, while details can be found in [14]. Therefore, a switching decoding scheme was used, where the switching variable (i.e. the measure of alignment for a given arm configuration) was controlling which of the models to be used for each configuration.

The original data set collected from each subject during the previously described experiments was used for training. After collecting the training data, each subject was asked to perform some new force tasks in ten different points in the 3D arm workspace, lasting about 5 seconds each. The switching decoding method was tested using those new experiments. The decoding method results are shown in Fig. 5. As it can be seen, the force estimates were close to the real ones measured for each of the 10 points that spanned a wide portion of the arm workspace. The root mean squared error (RMSE) and the correlation coefficient (CC) between the estimated and the real ones are also reported in Table I. The same criteria are computed using a single decoding model for all cases, i.e. without taking into consideration

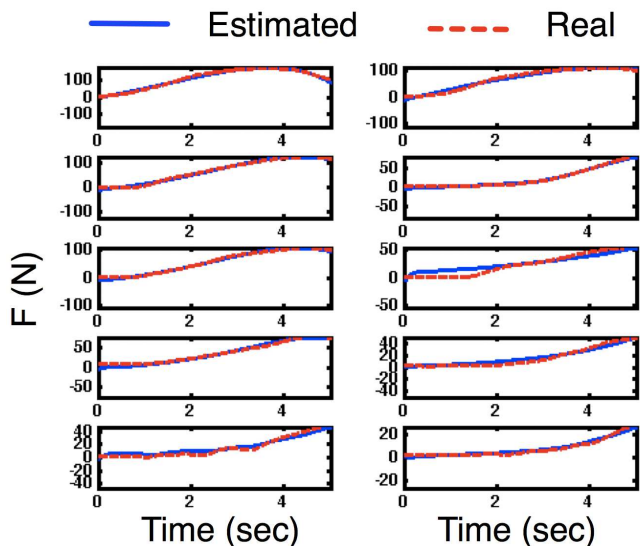


Fig. 5. Results on decoding 3D force magnitude from EMG recordings using the proposed method. Real and estimated values for force magnitude are shown for the subject's hand being in 10 different points in the arm workspace.

TABLE I

ACCURACY IN ESTIMATING HUMAN ARM EXERTED FORCES WITH THE PROPOSED SWITCHING METHODOLOGY AND A SINGLE DECODING MODEL.

Decoding model	CC	RMSE (N)
Switching	0.97	4.09
Single	0.78	14.23

the effect of the manipulability in muscle activation and in general the recruitment of the musculoskeletal system in force exertion tasks. These values are also included in Table I for comparison. As it can be seen, the information regarding the arm manipulability in the decoding process significantly improved the overall accuracy.

At this point, it must be noted, that although the 3D points in the workspace used for testing were selected by the subjects, their arm configuration and the direction of the exerted force were recorded and used for computing the manipulability information and alignment measure. However, this does not severely affect the applicability of the method, since in cases of worn devices (i.e. arm exoskeletons), this kind of information (i.e. arm configuration) is usually available through the device's sensors. Finally, all results presented are from subject 1, however they were also confirmed by subject 2 who showed very similar behavior.

#### IV. CONCLUSIONS AND DISCUSSION

In this paper, the arm force manipulability and its effect on the recruitment of the musculoskeletal system in arm force tasks was analyzed. It was shown that the axes of the manipulability ellipsoid play a significant role on the activation of the muscle while the arm is interacting with the environment, i.e. exerting forces to it. The main novelty of this paper is that for the first time, the human arm

manipulability is analyzed with respect to the force exerted and the muscle activations. Moreover, a decoding scheme is proposed that can estimate a continuous representation of the exerted force magnitude using the muscle activation as described by the surface electromyogram.

The proposed scheme could be used for controlling devices that are coupled or worn by humans for tasks involving force exertion to the environment. Until now, most of the studies have focused on the interaction between the human and the worn device. However, as the applications of the coupled human-robot devices are increasingly emerging in various fields (i.e. medical devices, rehabilitation robots, prosthetic devices), the need of the control of the interaction with the environment entailing contact forces is greater than ever before. Nevertheless, the proposed decoding scheme could be used for the control of arm exoskeletons during force tasks. Although the use of EMG signals as **control** interface has been proposed in the past, it has never been realized in orthotic devices that interact with the environment. In this paper, the effect of arm manipulability, which essentially depends on the arm configuration, was analyzed, while a robust method for using the electromyogram for the control of such devices was proposed.

#### REFERENCES

- [1] D. Shin, J. Kim, and Y. Koike, "A myokinetic arm model for estimating joint torque and stiffness from EMG signals during maintained posture," *J Neurophysiol*, vol. 101, pp. 387–401, 2009.
- [2] R. Osu, D. W. Franklin, H. Kato, H. Gomi, K. Domen, T. Yoshioka, and M. Kawato, "Short- and long-term changes in joint co-contraction associated with motor learning as revealed from surface EMG," *J Neurophysiol*, vol. 88, pp. 991–1004, 2002.
- [3] P. K. Artemiadis and K. J. Kyriakopoulos, "Estimating arm motion and force using emg signals: On the control of exoskeletons," *Proc. of IEEE/RSJ Int. Conf. Intelligent Robots and Systems*, pp. 279–284, 2008.
- [4] F. M. M. O. Campos and J. M. F. Calado, "Approaches to human arm movement control—a review," *Annual Reviews in Control*, vol. 33, pp. 69–77, 2009.
- [5] L. Sciavicco and B. Siciliano, *Modeling and control of robot manipulators*. McGraw-Hill, 1996.
- [6] P. K. Artemiadis, P. T. Katsiaris, and K. J. Kyriakopoulos, "A biomimetic approach to inverse kinematics for a redundant robot arm," *Autonomous Robots*, vol. 29(3), pp. 293–308, 2010.
- [7] N. A. Mpompos, P. K. Artemiadis, A. S. Oikonomopoulos, and K. J. Kyriakopoulos, "Modeling, full identification and control of the mitsubishi PA-10 robot arm," *Proc. of IEEE/ASME International Conference on Advanced Intelligent Mechatronics, Switzerland*, 2007.
- [8] F. E. Zajac, "Muscle and tendon: Properties, models, scaling, and application to biomechanics and motor control," *Bourne, J. R. ed. CRC Critical Rev. in Biomed. Eng.*, vol. 17, pp. 359–411, 1986.
- [9] J. R. Cram and G. S. Kasman, *Introduction to Surface Electromyography*. Inc. Gaithersburg, Maryland: Aspen Publishers, 1998.
- [10] G. McLachlan and D. Peel, *Finite mixture models*. John Wiley & Sons, Inc, 2000.
- [11] P. K. Artemiadis and K. J. Kyriakopoulos, "EMG-based control of a robot arm using low-dimensional embeddings," *IEEE Transactions on Robotics*, vol. 26(2), pp. 393–398, 2010.
- [12] I. T. Jolliffe, *Principal component analysis*. New York, Berlin, Heidelberg: Springer, 2002.
- [13] H. Akaike, "A new look at the statistical model identification," *IEEE Transactions on Automatic Control*, vol. 6, pp. 716–723, 1974.
- [14] P. K. Artemiadis and K. J. Kyriakopoulos, "A switching regime model for the EMG-based control of a robot arm," *IEEE Transactions on Systems, Man, and Cybernetics, Part B: Cybernetics*, vol. 99, pp. 1–11, 2010.